Nano Today 43 (2022) 101420

Contents lists available at ScienceDirect

Nano Today

journal homepage: www.elsevier.com/locate/nanotoday

Biomimetic confined self-assembly of chitin nanocrystals

Peiwen Liu[a,b,1], Jiaxiu Wang[c,d,b,1], Houjuan Qi[b,e,1], Tim Koddenberg[f], Dan Xu[b], Siyuan Liu[b], Kai Zhang[b,*]

[a] College of Engineering, Huazhong Agricultural University, Wuhan 430070, China
[b] Sustainable Materials and Chemistry, Department of Wood Technology and Wood-based Composites, University of Göttingen, Büsgenweg 4, D-37077 Göttingen, Germany
[c] School of Life Sciences, Anhui University, Hefei 230601, Anhui, China
[d] Anhui Key Laboratory of Modern Biomanufacturing, Hefei 230601, Anhui, China
[e] Key Laboratory of Bio-based Material Science & Technology, Ministry of Education, Material Science and Engineering College, Northeast Forestry University, Harbin 150040, China
[f] Wood Biology and Wood Products, University of Göttingen, Büsgenweg 4, D-37077 Göttingen, Germany

ARTICLE INFO

Article history:
Received 30 November 2021
Received in revised form 7 January 2022
Accepted 23 January 2022
Available online 29 January 2022

Keywords:
Self-assembly
Chitin nanocrystals
Confined geometry
Fixed-boundary
Tactoids

ABSTRACT

It is a longstanding challenge to aptly describe the natural assembly process of chitin Bouligand organization as well as biomimetic construct these position-dependent structures with the isolated chitin nanodomains. Here, we report a fixed-boundary evaporation-induced self-assembly (FB-EISA) modality using chitin nanocrystals (ChNCs) in the capillaries, where the generation of continuous and ordered anisotropic phase relies on the growth of phase boundary towards the opposite direction of water evaporation. Distinct from the previous EISA modalities with the moving evaporation interface, the pinned air-liquid interface at the end of capillaries in a confined environment acts as the evaporation interface and initial deposition site of ChNCs simultaneously. During the whole self-assembly process via successive evaporation, the generation of droplets-like ChNCs clusters known as tactoids is suppressed. Therefore, continuous birefringent multi-layers as nested multiple paraboloid structures of ChNCs with a density gradient are gradually generated, before cylindrical tubes are formed finally. The FB-EISA process can be accelerated by heat and maintains stable regardless of vibration or different capillary opening directions relative to gravity direction. This FB-EISA modality in confined geometry allows rapid formation of ChNCs-based photonics-quality structure of larger length scales and enables us to deepen our understanding of the natural self-assembly process in diverse biological species.

Introduction

The fascinating self-assembly of the native elementary building blocks in the biological matrix leads to complex three-dimensional (3D) structures with various functionalities in nature [1,2]. One typical such 3D structure is the hierarchical Bouligand architecture formed by chitin as uniaxial fiber layers that assemble themselves periodically into a helicoidal pattern [3–5]. Because the refractive indexes are different in the directions of the long axis and perpendicular to the long axis of chitin fibers, these ordered Bouligand structures embedded in the matrix of lipids, proteins, and polyphenols constitute iridescent cuticles [5–7]. In order to prepare large scale photonics-quality structures that can mimic this fascinating feature of organisms [8–12], an enormous effort has been previously devoted to understanding these natural assembly processes of nanodomains [13–17]. In these studies, the user-friendly evaporation-induced self-assembly (EISA) has been widely used to controllably organize the bio-based one-dimensional (1D) nanostructured materials, such as chitin nanocrystals (ChNCs) and cellulose nanocrystals, on multiple length scales [18–22].

However, the ordered droplets-like clusters of these nanocrystals known as tactoids are generally randomly dispersed in the resulting products, which generates multidomain birefringent structures with random sizes, orientations, and colors [8,13,23,24]. These microstructures generally occur in evaporation systems, where evaporation area and the deposition site are two separate interfaces of the suspensions. A large body of previous works confirmed that the

* Corresponding author.
E-mail address: kai.zhang@uni-goettingen.de (K. Zhang).
[1] These authors contributed equally.

https://doi.org/10.1016/j.nantod.2022.101420
1748-0132/

generation of tactoids at the evaporation interface, the imperfect merging and the uncontrolled turbulence of tactoids during the movement from the evaporation interface to deposition substrate, further spinodal decomposition of nanocrystals on the top of randomly distributed tactoids led to the formation of random colors [13,24]. To control the orientation of tactoids to improve the order of nanocrystals in obtained materials [25–27], various correlated challenges in the traditional EISA process still persist, such as the long duration of the self-assembly process [8], uncontrollable procedures [25], the instability to perturbation [6], unpredictable and unreproducible color in obtained materials [24].

Different than the position-dependent varying organization of ChNCs with the gradient distribution in the insects and various fruits [5,28], only plain chiral pseudo-layers of ChNCs that lay parallel to the evaporation interface in the intermediate and final state of the self-assembled structures were obtained from the artificial EISA processes so far [27,29,30]. These existing EISA modalities cannot be used to aptly describe the natural assembly process that always happens in the non-static environment. Compared to artificial self-assembled structures, the periodic polygonal photonic architectures on the micro- and nanoscale constitute the variety of iridescent cuticles in living organisms, e.g. beetles [5,28], while no obvious tactoid is known during their formation and growth.

Inspired by these native phenomena, we found that the rapid and biomimetic self-assembly of ChNCs into well-defined Bouligand structures in the confined geometry-capillaries underwent a gradual and sequential phase transition during the deposition of ChNCs with the presence of only one fixed phase boundary for the evaporation. The random generation of tactoids of ChNCs in the isotropic phase was suppressed, while the unique spatial variation of microstructure in the chiral nematic liquid crystal phase of ChNCs (as an anisotropic phase) showing novel birefringence domains was detected. This is opposite to commonly observed self-assembly modalities, in which the growth, coalescence and sedimentation of tactoids happened simultaneously.

Results and discussion

In the present work, ChNCs with the size of 241.8 ± 80 nm × 12.2 ± 5 nm (length×diameter) were isolated from shrimp chitin via alkaline periodate oxidation as described in the Methods (Supplementary Information Fig. S1) [31]. Aqueous suspension of 2 wt% ChNCs with a pure isotropic phase was used, where the spontaneous nucleation of ChNCs was not observed before the initial evaporation (Supplementary Information Fig. S2). Glass capillaries with inner diameters d of 0.4 and 0.9 mm were preferentially used as container to mimic the confined geometry of the periodic polygonal photonic units in the cuticles of insects. Round-shaped capillaries were chosen to minimize the impact of the inner surface of the capillaries on the FB-EISA of ChNCs. Similar FB-EISA process was also observed in the rectangle capillaries, although the final colors were slightly different (Supplementary Information Fig. S3).

The suspension of ChNCs was filled into the glass capillaries by capillary action. The filling length was set as 3.0 ± 0.1 cm, which enabled the formation of a solid structure with sufficient ChNCs and allowed for monitoring the birefringence evolution over a relatively short period. Another end of capillaries was filled with silicone oil to prevent evaporation at the air-liquid interface (I2) that is located in the middle of capillaries (Fig. 1A). Then, the capillaries filled with ChNCs were placed horizontally and dried under ambient conditions. In the present system, the evaporation interface (I1) stayed pinned at the open end of capillaries during the whole evaporation process and I1 also acted as the initial free-standing deposition area for ChNCs. As the water evaporated from I1 as a fixed boundary, I2 as the solid/liquid interface involving the gradual deposition of ChNCs was moving toward I1 (Fig. 1A-A1). These behaviors are distinct from the previously reported EISA processes, in which the water evaporation and deposition are towards two opposite directions and the evaporation interface is generally moving to the deposition interface (Fig. 1A-A2). For instance, if the other end of capillaries is completely sealed with wax, the self-assembly process resembled the conventional solvent casting process. Abundant tactoids were generated in suspensions of ChNCs within the 0.9 mm-capillaries after 24 h evaporation and clusters of ChNCs formed near the evaporation interface within the 0.4 mm-capillaries (Supplementary Information Fig. S4).

In contrast, the random generation of tactoids or clusters in the isotropic suspensions was suppressed during the FB-EISA in the capillaries, as depicted as dark regions in polarized optical microscopy (POM) images (Fig. 1B, Supplementary Information Fig. S3 and S5). The gradual water evaporation from I1 continuously increased the length of bright regions with longer time, which grew from the pinned air-liquid interface I1 as shown in POM images. The evolution of the birefringent domains via the water evaporation gradually generated ordered Bouligand structures of ChNCs in the capillaries with d = 0.4 and 0.9 mm (Fig. 1B, Supplementary Information Fig. S5).

The birefringent color near the center of I1 appeared initially white (1 min, Fig. 1B) and unique birefringent multi-layer domains as tubes were observed with POM starting from 0.5 h evaporation. The birefringent color near the center of I1 turned during a total evaporation period of 5.5 h from white to brown yellow, red, greenish blue, sea green, orange, brown, and so forth (Fig. 1C, Supplementary Information Fig. S6). Simultaneously, these colors at the interface I1 expanded horizontally from the center to the outer layers and formed birefringent onion-like multi-walled domains. Different than previous studies in which the confined evaporation air-liquid interface reached their final stabilized states in a relatively short period [29,30], the continuous evolution of birefringent colors at I1 in FB-EISA process exhibits a characteristic dynamic state during the whole evaporation process (Fig. 1B and C). When this continuous and well-defined birefringent domain reached the maximal length, the sequence of color variations accurately corresponds to the Michel-Lévy interference color chart [32], up to the third and seventh order in the capillaries of d = 0.4 and 0.9 mm, respectively (Fig. 1D, Supplementary Information Fig. S5). The change between different birefringent colors was clear and smooth (Fig. 1D and E).

With the gradual water evaporation after 5.5 h in the 0.4 mm-capillaries, the birefringent multi-layer tube structures reached the maximal length and the whole ChNC suspension was fixed in an ordered phase (Fig. 1B). With further water evaporation, the birefringent multi-layer hemicapsule-like and tube structures were continuously compressed. The layer number represented by the colors in this birefringence domain gradually reduced with proceeding evaporation (Fig. 1B), until the condensed phase was torn into dried pieces showing uniform colors. It is noteworthy that tactoids or the heterogeneous cluster of ChNCs were neither observed in the isotropic nor in the anisotropic phase in the capillaries with d = 0.4 or 0.9 mm, as indicated by the continuous dark areas in POM images (Fig. 1B, G, H, I, Supplementary Information Fig. S5). This behavior is comparable with the characteristic of the natural formation of Bouligand structures in living organisms. Besides, the shape of the phase boundary was not a straight plane as usual [29,30], and the areas close to the capillary wall were curved towards the fixed tube side (Fig. 1H and I, Supplementary Information Fig. S5).

The uniform and regular birefringent tube structures display the formation of the ordered Bouligand structure of ChNCs during the FB-EISA process. The microstructure of the birefringent multi-layer domains at the intermediate state and final state were investigated

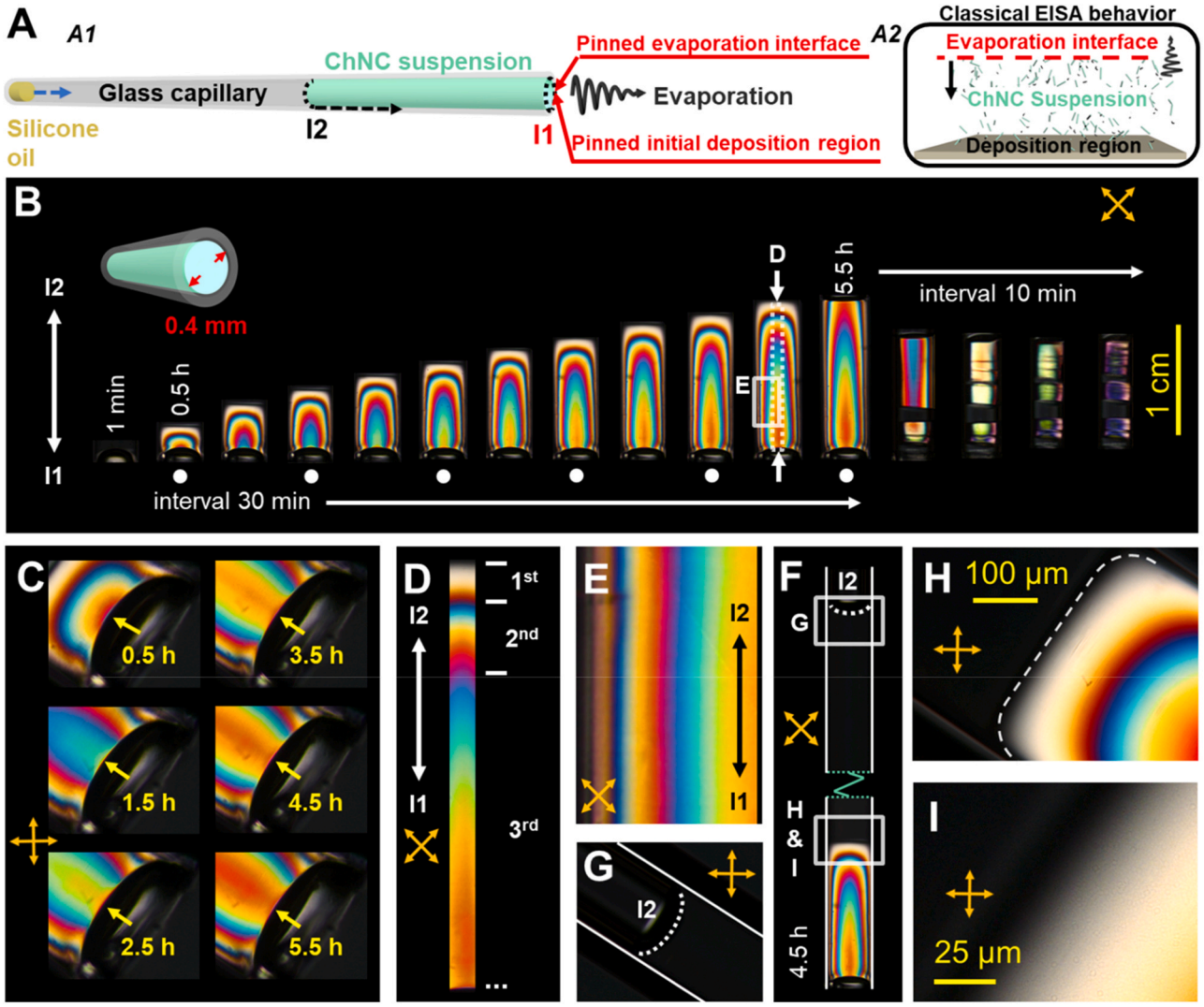

Fig. 1. The evolution of the birefringent domains during the confined FB-EISA process of ChNCs. A) Schematic representation of the experimental set-up for the confined FB-EISA of ChNCs (*A1*) and the representative behavior of the slip evaporation interface in classical EISA process (*A2*). B) The representative polarized optical microscopy (POM) images for the evolution of the birefringent domains in a capillary with the inner diameter of 0.4 mm. C) Enlarged view of the color evolution of the interface I1 with times. D) and E) The multi-orders of birefringence domains formed in the axial direction near the center and wall of the capillary, respectively, as marked in B. F) The representative POM image of the isotropic and anisotropic phases. G) POM image of the interface I2. H) and I) POM images showing the isotropic and anisotropic phase boundary with different magnifications.

(Fig. 2A). In the capillaries with d = 0.4 and 0.9 mm, the birefringent multi-layer hemicapsule-like domains at the near maximal length after 5 h evaporation were freeze-dried. Spatial variation of the microstructure with gradient densities was found in the obtained solid structure, as displayed by XμCT slice images (Fig. 2B, Supplementary Information Fig. S6 and S7). The density of ChNCs layers showed gradient in both the longitudinal section and the cross-section (Figs. 2B, C and D, Supplementary Information Fig. S6). Specifically, the density of the ChNCs layers decreased in the longitudinal section along the growth direction of the birefringent domains (I1 to I2), while the density of ChNCs layers in the transverse direction becomes higher from the centre to the edge. The centre area contained the isotropic phase that existed still as the suspension of ChNCs and presented after drying as dark areas with porous structure due to the low amount of ChNCs, as can be observed from the XμCT slice images and SEM image (Fig. 2B, C and D). Moreover, more suspension was present close to I2 before drying as shown by larger dark area, while the centre area close to I1 was already solidified with completed layers. The pores in the isotropic areas after drying are generally aligned along the longitudinal axis of the capillary.

Therefore, the ordered structure within the cylindrical tubes of ChNCs formed during the FB-EISA process is a continuous alternating structure with a gradient density (Figs. 2B and D). Diverse regions are present: S1) continuous ChNCs layers perpendicular to the capillary wall in the region close to I1, S2) the elliptic paraboloid ChNCs layers opening toward I1 in the middle of the ChNCs cylindrical fiber, and S3) region with the coexistence of the anisotropic and isotropic phase near I2. The region in S3 contains the annular hollow paraboloid ChNCs layers which opened toward I1. These annular hollow paraboloid ChNCs layers in S3 were formed by converting the isotropic phase as ChNC suspension into the anisotropic phase during drying. With further evaporation to 5.5 h, region S3 with the coexisting anisotropic and isotropic phase was primarily converted into the elliptic paraboloid ChNCs layers as in S2 opening toward I1 due to the continuous loss of water and deposition of ChNCs (Supplementary Information Fig. S8). Thus, these position-dependent varying organization of ChNCs layers with the gradient distribution in this artificial EISA process can address the goal of biomimetic design of insect cuticles, in which the pitch length and the helical axis orientation must be position-dependent across the material [5,28].

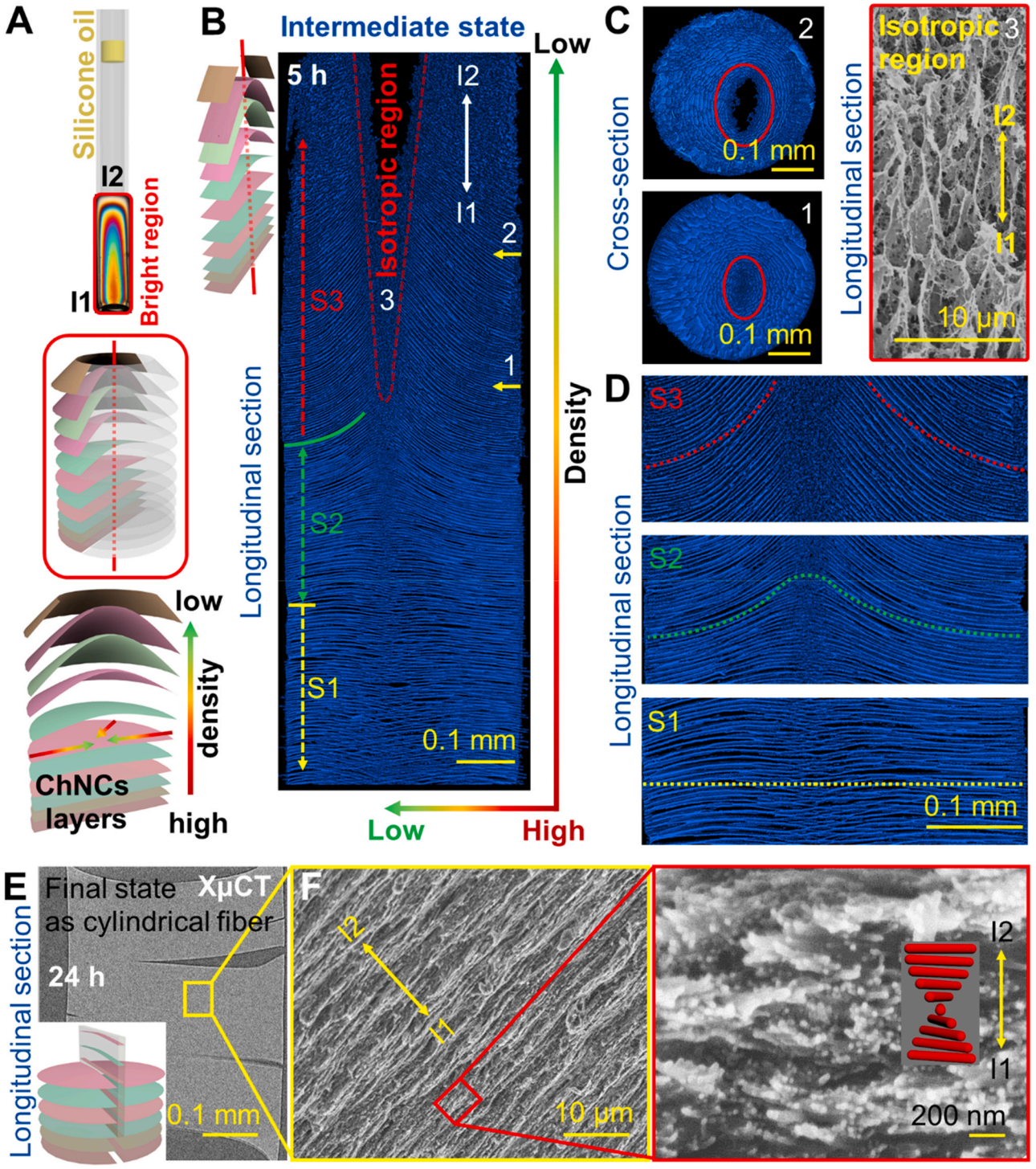

Fig. 2. Spatial variation of microstructure evolution during the confined FB-EISA process of ChNCs. A) Schematic representation for the spatial variation of microstructure in the longitudinal section. B) X-ray micro-computed tomography (XμCT) slice image showing the representative longitudinal section morphology of the gradient anisotropic phase. The markers correspond approximately to regions of the different structures and measurement positions, at which the microstructures in Fig. C and D were obtained. C) Cross-section of the coexistence region of isotropic and anisotropic phase. The dark region within the red circles in the center of the cross-section 1 and 2 are the low-density isotropic phase. SEM image shows the longitudinal section of the isotropic phase in the coexistence region 3. D) XμCT slice images of three representative microstructures in the longitudinal section. E) XμCT slice image (without visualization) and F) SEM images of the dried cylindrical tube of ChNCs in the longitudinal section and the characteristic Bouligand structure.

At the end of evaporation of 24 h, a dense and parallel ChNCs multilayer was observed in the cylindrical tubes of ChNCs (Fig. 2E). The left-handed Bouligand character was found in the longitudinal section, and the pitch height is nearly 1.4 μm (Fig. 2F). Moreover, the control experiments ruled out the formation of these multi-layer structures because of ice-templating of ChNC suspensions, because the direct freeze-drying of ChNC suspensions only led to porous structures (Supplementary Information Fig. S9).

Based on aforementioned results, confined FB-EISA process of ChNCs in round capillaries should proceed as shown in Fig. 3. Initially, the accumulation of ChNCs in the meniscus (I1) is induced by water evaporation (Fig. 1B, Supplementary Information Fig. S5). ChNCs are oriented parallel to the contact line but perpendicular to

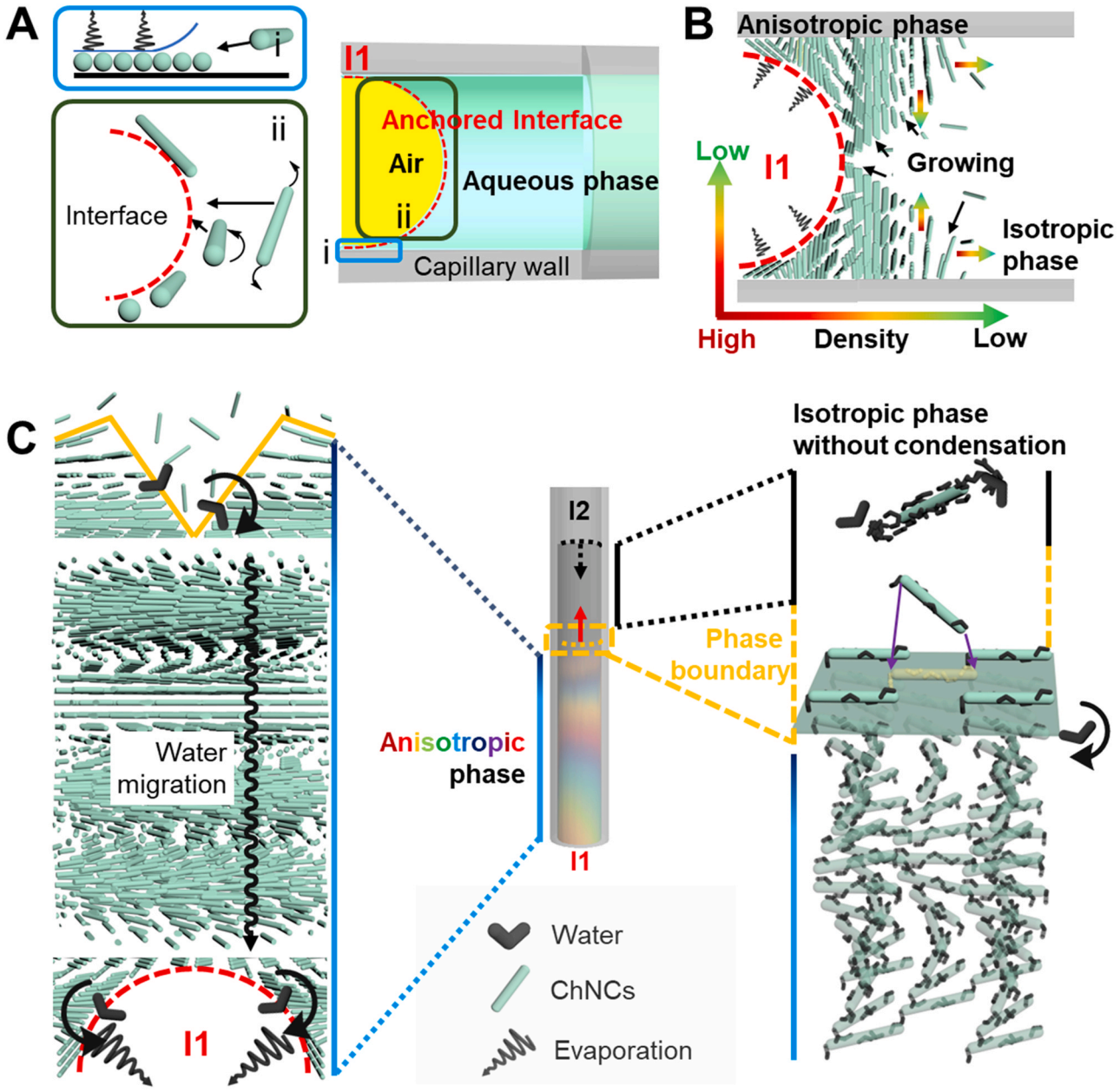

Fig. 3. Schematic representation for the proposed FB-EISA process of ChNCs in round capillaries. A) Depiction of the deposited ChNCs at the interface I1 of air and water. B) Illustration of the initial growing process of the anisotropic phase. C) Migration of the water during the FB-EISA process and self-assembly of ChNCs at the phase boundary between assembled structure and isotropic suspension.

the long axis of the capillary tube in the evaporating meniscus to maximize the interfacial coverage (Fig. 3A, Supplementary Information Fig. S10 and S11). The air-liquid interface I1 was pinned due to the deposition of ChNCs during the whole self-assembly process (Fig. 1B). Simultaneously, ChNCs tended to adsorb initially at the air-liquid interface (I1) (Supplementary Information Fig. S11) to minimize their interface attachment energy [33]. After the formation of the first layer of ChNCs, ChNCs in the isotropic region self-assembled on the inner surface of this ChNC layer, when water in the isotropic phase migrated to the neighboring evaporating meniscus. At the same time, ChNCs were accumulated in evaporating meniscus and deposited preferentially near the capillary wall, leading to the anisotropic phase with a density gradient from the center to the wall (Fig. 3B). Following this, initial, slightly deformed annular hollow paraboloid ChNCs layers were formed with the opening toward the air-liquid interface I1. Moreover, the anisotropic phase should grow from the wall toward the core of the capillaries in the radiate direction due to the initial possible deposition of ChNCs and from air-liquid interface I1 toward I2 in the longitudinal direction (Fig. 3B).

It is noteworthy that the concentration-induced phase transition only happened near the phase boundary between the assembled structure and the isotropic ChNC suspension (Fig. 3C, Supplementary Information Fig. S13). Water from the suspension should firstly migrate through the anisotropic phase to evaporate, and then water in the anisotropic phase of cylindrical tube of ChNCs will be continually squeezed out from the multi-layer structure by the evaporation from I1 (Fig. 3C). Subsequently, multi-layer structure as S1 in the regions close to I1 was formed at first (Figs. 2B and 2D). The residual cylindrical tube of ChNCs underwent the formation of coexisting region of isotropic and anisotropic ~~regions~~ phase as S3, then S2 as paraboloid ChNCs layers and finally only solid cylindrical tubes of ChNCs with a dense multi-layer structure (Fig. 2E).

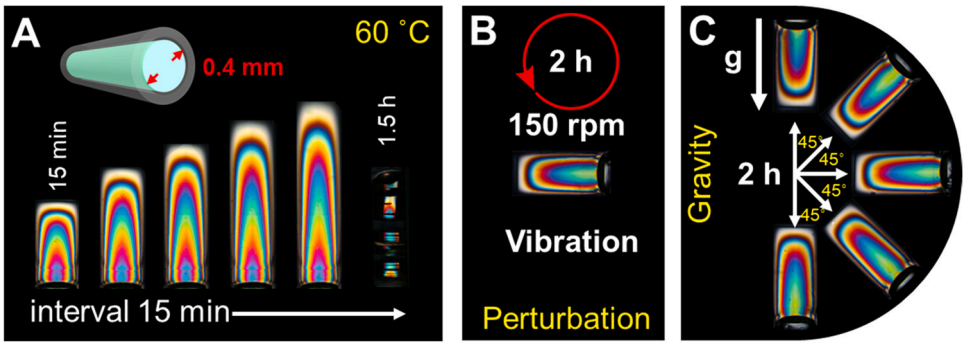

Fig. 4. Stable confined FB-EISA process of ChNCs. POM images showing the birefringent domains formed in capillaries with A) heating at 60 °C, B) vibration of 150 rpm for 2 h and C) various directions of capillaries.

With overlapped and anchored evaporation interface and initial deposition substrate at I1, the confined FB-EISA process of ChNCs in the 0.4 mm-capillaries was highly stable. The evolution of the birefringent domains underwent equal process, even when placed in surroundings with higher temperatures, perturbation, and changing direction of capillaries (Fig. 4). Faster water evaporation caused by heating even significantly accelerated the FB-EISA process of ChNCs and the reproducible birefringent evolution was generated in capillaries (Fig. 4 A, Supplementary Information Fig. S14). It took 1.5 h and 3 h to complete the whole birefringent evolution in the 0.4 mm-capillaries at 60 °C and 40 °C, respectively. In contrast, the same evolution took nearly 6 h at room temperature (Fig. 1B). It should be noted that the temperature fluctuation during the FB-EISA process caused the mutation of structural colors due to the sudden change of evaporation rate (Supplementary Information Fig. S14).

Furthermore, the birefringent domains in 0.4 mm-capillaries were still consistently formed as under static conditions, even when the capillaries were vibrated at 150 rpm for 2 h (Fig. 4B). As well, the FB-EISA process was not affected with the capillaries placed with various angles compared to the direction of gravity of 180°, 135°, 90°, 45°, and 0° (Fig. 4C), except for the slight difference in the length of the birefringent domains. In contrast, the ChNC suspension in the 0.9 mm-capillaries could not stay pinned at the end of the capillaries during the vibration and changing the direction of capillaries. This should be due to the smaller ratio of the contact area compared to the volume of the ChNC suspension. If the FB-EISA in 0.9 mm-capillaries was performed under the static conditions for 1 h at the beginning, the evolution of the birefringent domains became stable regardless of heating, perturbation, and changing of the direction of capillaries during the further evaporation. Therefore, the formation of an initial stabilized interface for both evaporation and deposition, which needs 1 h for 0.9 mm-capillaries and starts directly for 0.4 mm-capillaries due to their different opening size is critical for setting out the stable FB-EISA.

This rapid and facile FB-EISA of ChNCs into the well-defined structure in capillaries undergo the phase transition from the isotropic ChNC suspension to the anisotropic in cylindrical tubes, which only occurs at the regions near the non-planar phase boundary. The typical nucleation of the nanocrystals to tactoids in the isotopic phase during the existing EISA processes [13] was not observed in this new FB-EISA. Compared to previous EISA processes which are generally very sensitive to subtle environmental change, the present FB-EISA process is for the first time highly robust by showing the excellent stability against heating, vibration, and directions of capillary opening. Within this confined FB-EISA process, the density and the helical axis orientation of the self-assembled structures were position-dependent across the cylindrical tubes of ChNCs. In addition, the unique birefringent multi-layer hemicapsule-like domains as tubes were generated, as the water gradually evaporated from the ChNC suspension.

This novel self-assembly process is mainly attributed to the confined geometry and the unique evaporation system, in which the pinned air-liquid interface at the end of capillaries acts as the evaporation interface and initial deposition substrate simultaneously. By using square capillaries for the FB-EISA under otherwise equal conditions, similar color variations and the birefringent domains were also obtained and therefore ruled out the shape of the capillary as the only reason (Supplementary Information Fig. S3 and S15). Therefore, the successive conduction of water from the isotropic to the anisotropic phase and the water evaporation from the fixed boundary primarily generated the ChNCs layers with a density gradient and the nested paraboloid structure of ChNCs as unique birefringent domains.

After the formation of the interface as fixed evaporation boundary and deposition substrate, the evaporation of the water in the isotropic phase needs the water molecules to migrate through the anisotropic phase to I1 (Fig. 3C). Simultaneously, ChNCs in the isotropic phase undergo the phase transition and are deposited on the exiting anisotropic phase, which only happens in the regions near the non-planar phase boundary I2. Therefore, the concentration in the isotropic phase is inhabited and the water migration enables the isotropic phase to remain in a dynamic state. Following this, the formation of tactoids in the isotropic phase is prevented, as long as water continuously migrates out of capillaries and evaporates from the interface I1.

Globally, during the EISA in previous reports or the general nucleation process of nanoparticles, the evaporation interface and deposition substrate are always separated (Fig. 1A and 5) [34]. The isotropic suspension is located between them and the evaporation interfaces are in a state of steady movement until complete drying. The heterogeneous structures are formed during the coalescence of the randomly nucleated clusters that sediment from the suspension on the deposition substrate. In parallel, the nanoparticles undergo phase transition because of the water evaporation and also deposit on the deposition substrate as continuously ordered fractions. In these EISA processes, water migrates from the highly ordered fractions from the deposition substrate after the suspension is evaporated (Fig. 5A), while FB-EISA relies on the water migration from the suspension toward the deposition substrate for the evaporation (Fig. 5B).

To our best knowledge, only two previous studies reported similar systems which were performed in rectangular capillary or in the space between two glass sheets [29,30]. However, the resulting birefringent domains and microstructures of the self-assembled structures were plain planar. The multidomain birefringent structures with random orientations and colors still represented conventional EISA processes, while FB-EISA was not revealed. However, simple and effective production of the large area containing uniform birefringent regions of ChNCs via the present FB-EISA process would be a challenge for their application. Being inspired by iridescent

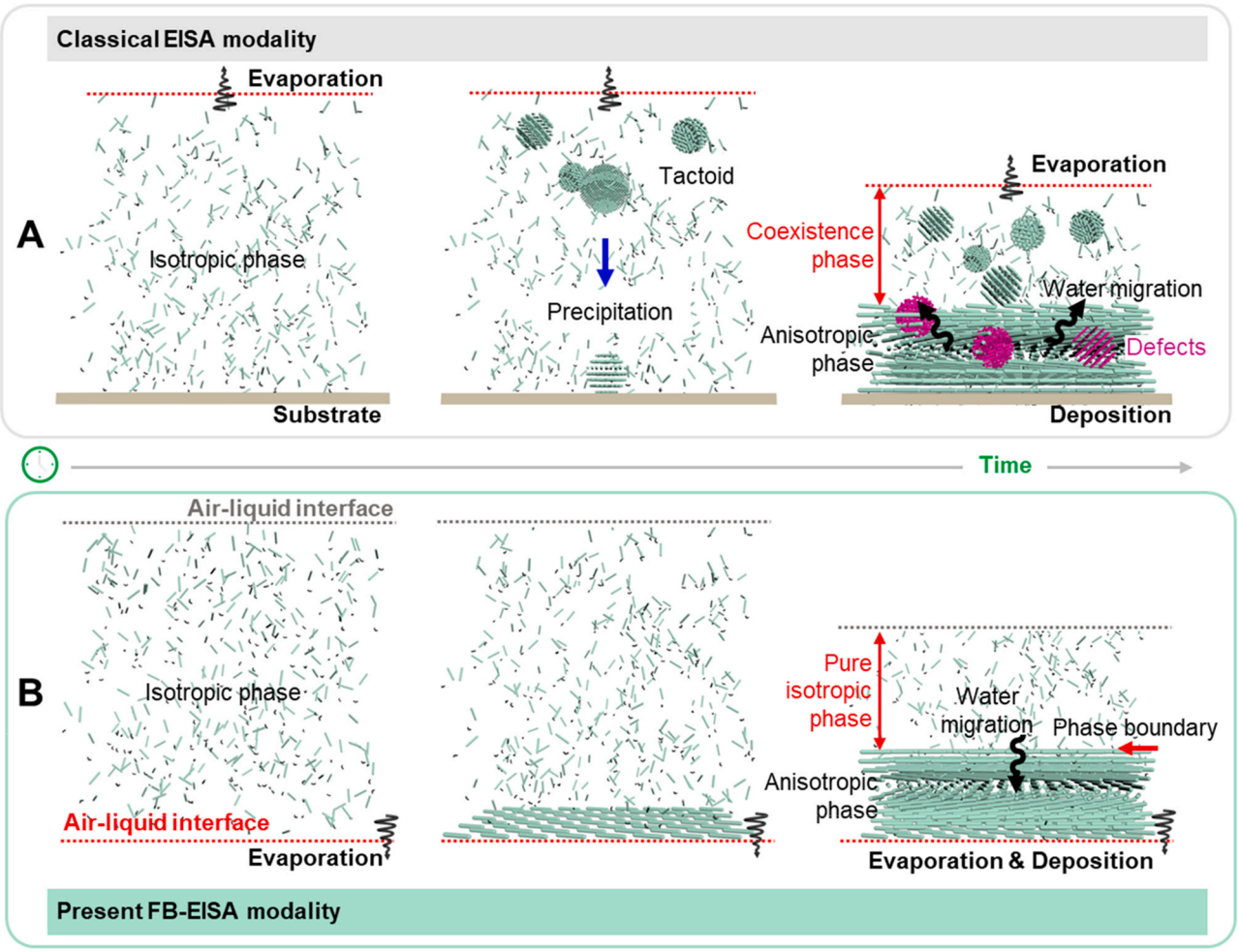

Fig. 5. Comparison between the classical EISA (A) and the present FB-EISA process (B).

cuticles of beetles which are formed by the arrangement of the periodic polygonal photonic architectures on the nano- and micro-scale, use of substrates containing well-defined nano-/micro-structures, e.g. capillaries array, could induce the spatial arrangement of ChNCs in large areas. Such substrates will enable ChNCs to comply with FB-EISA in the confined geometry and finally to form large-area Bouligand structures.

Conclusion

To conclude, FB-EISA generates ordered and uniform multi-layer structures of ChNCs without formation of tactoids via the fixed-boundary interface for both evaporation and deposition, while previous reports of the classical EISA process involve the growth, coalescence and random sedimentation of tactoids, the separated interfaces as the moving evaporation interface and deposition interface. In contrast to existing EISA, the iconic features of the present FB-EISA modality are: (1) the pinned air-liquid interface acts as the evaporation interface and initial deposition substrate simultaneously, (2) the evaporation surface is fixed and the anisotropic phase grows toward an opposite site, thereby suppressing of formation of tactoids, while the evaporation surface in conventional EISA is constantly moving and the anisotropic phase grows toward the evaporation surface, (3) the evaporation of water in the isotropic phase needs to migrate through the anisotropic phase and thereby causes the phase change of ChNCs at the solid-liquid interface I2, while water evaporates from the solution surface in the conventional EISA without permeating the anisotropic phase. This work introduces a new class of EISA modality and possibly provides the basis for aptly understanding the natural assembly process of chitin, which will expand the method and strategy for the preparation of biomimetic structures, macromolecular crystals, templates and larger length scales photonics-quality structures for nanotechnology.

CRediT authorship contribution statement

P.L. and K.Z. conceived the project and designed the experiments. P.L., J.W. and H.Q. conducted most of the experiments. T.K. and P.L. discussed and conducted X-ray micro-computed tomography. P.L., J.W., H.Q., D.X., S.L., and K.Z. wrote most of the manuscript. All authors discussed the results and contributed to the final manuscript. written through contributions of all authors. All authors have given approval to the final version of the manuscript.

Declaration of Competing Interest

The authors declare that they have no known competing financial interests or personal relationships that could have appeared to influence the work reported in this paper.

Acknowledgment

K.Z. and P.L. thank the Federal Ministry for Economic Affairs and Energy (BMWi, Germany) and the Ministry for Science and Culture of Lower Saxony (MWK, Germany) for the financial support of WIPANO project (FKZ03THW05K14). J.W., H.Q., D.X. and S.L. thank

China Scholarship Council (CSC, China) for the financial support. We thank Prof. Dr. Oliver Bäumchen from Max Planck Institute for Dynamics and Self-Organization, for the inspiring discussion and the great support during finishing this paper. We cordially thank Mrs. Xiaolin Ding from the University of Göttingen for providing water-color painting of shrimp in supporting information.

Appendix A. Supporting information

Supplementary data associated with this article can be found in the online version at doi:10.1016/j.nantod.2022.101420.

References

[1] U.G.K. Wegst, H. Bai, E. Saiz, A.P. Tomsia, R.O. Ritchie, Bioinspired structural materials, Nat. Mater. 14 (2015) 23–36.
[2] M. Eder, S. Amini, P. Fratzl, Biological composites—complex structures for functional diversity, Science 362 (2018) 543–547.
[3] J.C. Weaver, G.W. Milliron, A. Miserez, K. Evans-Lutterodt, S. Herrera, I. Gallana, W.J. Mershon, B. Swanson, P. Zavattieri, E. DiMasi, D. Kisailus, The stomatopod dactyl club: a formidable damage-tolerant biological hammer, Science 336 (2012) 1275–1280.
[4] W. Huang, M. Shishehbor, N. Guarín-Zapata, N.D. Kirchhofer, J. Li, L. Cruz, T. Wang, S. Bhowmick, D. Stauffer, P. Manimunda, K.N. Bozhilov, R. Caldwell, P. Zavattieri, D. Kisailus, A natural impact-resistant bicontinuous composite nanoparticle coating, Nat. Mater. 19 (2020) 1236–1243.
[5] A. Scarangella, V. Soldan, M. Mitov, Biomimetic design of iridescent insect cuticles with tailored, self-organized cholesteric patterns, Nat. Commun. 11 (2020) 4108.
[6] A. Tran, C.E. Boott, M.J. MacLachlan, Understanding the self-assembly of cellulose nanocrystals—toward chiral photonic materials, Adv. Mater. 32 (2020) 1905876.
[7] S. Vignolini, P.J. Rudall, A.V. Rowland, A. Reed, E. Moyroud, R.B. Faden, J.J. Baumberg, B.J. Glover, U. Steiner, Pointillist structural color in Pollia fruit, Proc. Natl. Acad. Sci. U.S.A. 109 (2012) 15712–15715.
[8] A.G. Dumanli, G. Kamita, J. Landman, H. van der Kooij, B.J. Glover, J.J. Baumberg, U. Steiner, S. Vignolini, Controlled, bio-inspired self-assembly of cellulose-based chiral reflectors, Adv. Opt. Mater. 2 (2014) 646–650.
[9] P. Rofouie, M. Alizadehgiashi, H. Mundoor, I.I. Smalyukh, E. Kumacheva, Self-assembly of cellulose nanocrystals into semi-spherical photonic cholesteric films, Adv. Funct. Mater. 28 (2018) 1803852.
[10] H. Liu, B. Pang, Q. Tang, M. Müller, H. Zhang, R. Dervişoğlu, K. Zhang, Self-assembly of surface-acylated cellulose nanowhiskers and graphene oxide for multiresponsive janus-like films with time-dependent dry-state structures, Small 16 (2020) 2004922.
[11] Q. Liu, M.G. Campbell, J.S. Evans, I.I. Smalyukh, Orientationally ordered colloidal Co-dispersions of gold nanorods and cellulose nanocrystals, Adv. Mater. 26 (2014) 7178–7184.
[12] K.E. Shopsowitz, H. Qi, W.Y. Hamad, M.J. MacLachlan, Free-standing mesoporous silica films with tunable chiral nematic structures, Nature 468 (2010) 422–425.
[13] P.-X. Wang, W.Y. Hamad, M.J. MacLachlan, Structure and transformation of tactoids in cellulose nanocrystal suspensions, Nat. Commun. 7 (2016) 11515.
[14] Y. Li, J. Jun-Yan Suen, E. Prince, E.M. Larin, A. Klinkova, H. Thérien-Aubin, S. Zhu, B. Yang, A.S. Helmy, O.D. Lavrentovich, E. Kumacheva, Colloidal cholesteric liquid crystal in spherical confinement, Nat. Commun. 7 (2016) 12520.
[15] R.M. Parker, B. Frka-Petesic, G. Guidetti, G. Kamita, G. Consani, C. Abell, S. Vignolini, Hierarchical self-assembly of cellulose nanocrystals in a confined geometry, ACS Nano 10 (2016) 8443–8449.
[16] J.P.F. Lagerwall, C. Schütz, M. Salajkova, J. Noh, J. Hyun Park, G. Scalia, L. Bergström, Cellulose nanocrystal-based materials: from liquid crystal self-assembly and glass formation to multifunctional thin films, NPG Asia Mater. 6 (2014) e80-e80.
[17] G. Nyström, M. Arcari, R. Mezzenga, Confinement-induced liquid crystalline transitions in amyloid fibril cholesteric tactoids, Nat. Nanotechnol. 13 (2018) 330.
[18] Y. Lin, E. Balizan, L.A. Lee, Z. Niu, Q. Wang, Self-assembly of rodlike bio-nanoparticles in capillary tubes, Angew. Chem. Int. Ed. 49 (2010) 868–872.
[19] Z. Zhao, H. Wang, L. Shang, Y. Yu, F. Fu, Y. Zhao, Z. Gu, Bioinspired heterogeneous structural color stripes from capillaries, Adv. Mater. 29 (2017) 1704569.
[20] C.J. Brinker, Evaporation-induced self-assembly: functional nanostructures made easy, MRS Bull. 29 (2011) 631–640.
[21] W. Han, Z. Lin, Learning from “Coffee Rings”: ordered structures enabled by controlled evaporative self-assembly, Angew. Chem. Int. Ed. 51 (2012) 1534–1546.
[22] K. Yao, Q. Meng, V. Bulone, Q. Zhou, Flexible and responsive chiral nematic cellulose nanocrystal/poly(ethylene glycol) composite films with uniform and tunable structural color, Adv. Mater. 29 (2017) 1701323.
[23] P.-X. Wang, M.J. MacLachlan, Liquid crystalline tactoids: ordered structure, defective coalescence and evolution in confined geometries, philosophical transactions of the royal society a: mathematical, Phys. Eng. Sci. 376 (2018) 20170042.
[24] B. Zhu, V.E. Johansen, G. Kamita, G. Guidetti, M.M. Bay, T.G. Parton, B. Frka-Petesic, S. Vignolini, Hyperspectral imaging of photonic cellulose nanocrystal films: structure of local defects and implications for self-assembly pathways, ACS Nano (2020).
[25] P.-X. Wang, W.Y. Hamad, M.J. MacLachlan, Liquid crystalline tactoidal microphases in ferrofluids: spatial positioning and orientation by magnetic field gradients, Chem 5 (2019) 681–692.
[26] B. Frka-Petesic, H. Radavidson, B. Jean, L. Heux, Dynamically controlled iridescence of cholesteric cellulose nanocrystal suspensions using electric fields, Adv. Mater. 29 (2017) 1606208.
[27] Y. Li, E. Prince, S. Cho, A. Salari, Y.M. Golestani, O.D. Lavrentovich, E. Kumacheva, Periodic assembly of nanoparticle arrays in disclinations of cholesteric liquid crystals, Proc. Natl. Acad. Sci. U.S.A. 114 (2017) 2137–2142.
[28] C. Bayon, G. Agez, M. Mitov, Wavelength-tunable light shaping with cholesteric liquid crystal microlenses, Lab Chip 14 (2014) 2063–2071.
[29] V. Cherpak, V.F. Korolovych, R. Geryak, T. Turiv, D. Nepal, J. Kelly, T.J. Bunning, O.D. Lavrentovich, W.T. Heller, V.V. Tsukruk, Robust Chiral Organization of cellulose nanocrystals in capillary confinement, Nano Lett. 18 (2018) 6770–6777.
[30] B.L. Tardy, J.J. Richardson, L.G. Greca, J. Guo, H. Ejima, O.J. Rojas, Exploiting supramolecular interactions from polymeric colloids for strong anisotropic adhesion between solid surfaces, Adv. Mater. 32 (2020) 1906886.
[31] P. Liu, H. Liu, T. Schäfer, T. Gutmann, H. Gibhardt, H. Qi, L. Tian, X.C. Zhang, G. Buntkowsky, K. Zhang, Unexpected selective alkaline periodate oxidation of chitin for the isolation of chitin nanocrystals, Green Chem. (2021).
[32] B.E. Sørensen, A revised Michel-Lévy interference colour chart based on first-principles calculations, Eur. J. Mineral. 25 (2013) 5–10.
[33] P. Liu, B. Pang, L. Tian, T. Schäfer, T. Gutmann, H. Liu, C.A. Volkert, G. Buntkowsky, K. Zhang, Efficient, self-terminating isolation of cellulose nanocrystals through periodate oxidation in pickering emulsions, ChemSusChem 11 (2018) 3581–3585.
[34] C. Sanchez, C. Boissière, D. Grosso, C. Laberty, L. Nicole, Design, synthesis, and properties of inorganic and hybrid thin films having periodically organized nanoporosity, Chem. Mater. 20 (2008) 682–737.